The Journal of Chemical Physics

# Full-quantum descriptions of molecular systems from constrained nuclear–electronic orbital density functional theory

Cite as: J. Chem. Phys. **153**, 074106 (2020); https://doi.org/10.1063/5.0014001
Submitted: 18 May 2020 . Accepted: 23 July 2020 . Published Online: 18 August 2020

Xi Xu, and Yang Yang



AIP Publishing

The Journal of Chemical Physics ARTICLE scitation.org/journal/jcp

# Full-quantum descriptions of molecular systems from constrained nuclear–electronic orbital density functional theory

Cite as: J. Chem. Phys. 153, 074106 (2020); doi: 10.1063/5.0014001
Submitted: 18 May 2020 • Accepted: 23 July 2020 •
Published Online: 18 August 2020



Xi Xu and Yang Yang[a)]

## AFFILIATIONS

Theoretical Chemistry Institute and Department of Chemistry, University of Wisconsin-Madison, 1101 University Avenue, Madison, Wisconsin 53706, USA

[a)]Author to whom correspondence should be addressed: yyang222@wisc.edu

## ABSTRACT

We develop a full-quantum formulation of constrained nuclear–electronic orbital density functional theory (cNEO-DFT). This formulation deviates from the conventional Born–Oppenheimer framework, and all nuclei and electrons are treated on an equal footing within the molecular orbital picture. Compared to the conventional DFT, the ground state energy in full-quantum cNEO-DFT inherently includes all vibrational zero-point energies. We also derived and implemented the analytic gradient of the full-quantum cNEO-DFT energy with respect to the quantum nuclear expectation positions. With the analytic gradient, the geometry optimizations are performed, which naturally include the nuclear quantum effects and describe the geometric isotope effects. The full-quantum cNEO-DFT is tested on a series of small molecules and the transition states of two hydrogen transfer reactions. The results are compared with those from conventional DFT, DFT-VPT2, and NEO-DFT with only key protons treated quantum mechanically. It is found that the nuclear quantum effects have notable impacts on molecular equilibrium geometries and transition state geometries. The full-quantum cNEO-DFT can be a promising method for describing the nuclear quantum effects in many chemical processes.



## I. INTRODUCTION

The Born–Oppenheimer (BO) approximation is the first approximation in conventional electronic structure theory and has been successful in describing a wide range of chemical phenomena and chemical processes. In the conventional BO picture, the nuclei are first treated as fixed point charges that provide an external potential for electrons, and the electrons are described by the wave function solved from the corresponding Schrödinger equation. Afterward, the energy obtained from the electronic Schrödinger equation can serve as the potential for the nuclei, based on which the nuclear wave function can be solved and the nuclear states can be described. The BO approximation is a valid approximation in most chemical processes due to the large nuclei/electron mass ratio and thus a significant time-scale difference for the motions of nuclei and electrons. However, it faces challenges in nonadiabatic processes, which often occur in the coordinate space where two potential energy surfaces are close in energy, for example, a conical intersection.[1]

Many theoretical methods have been developed to circumvent the problems related to the BO approximation.[2–6] The nuclear–electronic orbital (NEO) theory is one of them. In the NEO framework, both electrons and nuclei are treated simultaneously with the molecular orbital theory.[7–10] As a variant in the multicomponent quantum theory, its basic ideas and concepts have long been established,[11] and there has been important progress in both NEO wave function theory and NEO density functional theory (NEO-DFT) in the past two decades.[10] In the NEO framework, the nuclear quantum effects can be directly described by the orbital picture of the key nuclei, and the effects on both ground and excited states properties have been studied.[12–16] However, the conventional NEO framework has a big limitation, which is that at least two

nuclei need to be treated classically as point charges to fix the molecular frame and thus to avoid the difficulties with translations and rotations.[10] Consequently, simple diatomic molecules, such as $H_2$ and HF, cannot be described. Furthermore, although the BO separation between electrons and key quantum nuclei is avoided, the requirement of classical nuclei invokes a new BO separation between the quantum and classical nuclei.[17] This new BO separation may be even less reasonable compared to the original one because of the small mass difference among the nuclei. As a result, the vibrational frequencies calculated by NEO do not directly correspond to the vibrations observed in experiments,[17,18] and further applications to nonadiabatic dynamics might face even more challenges.

In our previous work, we developed the constrained NEO-DFT (cNEO-DFT) to obtain extended NEO energy surfaces that incorporate the nuclear quantum effects.[19] It is achieved by imposing a constraint on the expectation position of a specific key quantum nucleus without assuming that the quantum nucleus responds immediately to the motion of classical nuclei. In this paper, we generalize this theory and apply the constraint to all nuclei. In this way, all nuclei and electrons are described on the same footing with a full-quantum picture that completely deviates from the BO framework. Compared to conventional NEO-DFT, which requires at least two classical nuclei, the full-quantum cNEO-DFT overcomes the difficulties related to translations and rotations because the constrained expectation positions naturally fix the molecular frame. Additionally, we also derive and implement the analytic gradient of the full-quantum cNEO-DFT, making it applicable to geometry optimizations, transition state search, and potentially the studies of chemical dynamics in the future.

This paper is organized as follows: In Sec. II, we present the general formulation of full-quantum cNEO-DFT and its analytic gradient. Then, in Secs. III and IV, we use the analytic gradient of full-quantum cNEO-DFT to search for the equilibrium geometries of a series of small molecules and the transition states of two hydrogen transfer reactions. The results are compared with those from conventional DFT, DFT-VPT2,[20] and NEO-DFT with only the key proton treated quantum mechanically. Finally, we provide the concluding remarks in Sec. V.

## II. THEORY

### A. Full-quantum formulation of cNEO-DFT

The basic formulation of cNEO-DFT has been presented in our previous work.[19] In this section, the generalization to the full-quantum case is introduced, in which a constraint is imposed on the expectation position for every nucleus.

The theoretical foundation for non-Born–Oppenheimer density functional theory or multicomponent density functional theory has been laid about forty years ago by Capitani *et al.*[21] The ground state energy of the system is a functional of one-particle densities,

$$E_{\text{g.s.}} = E[\rho^e, \{\rho^{n_u}\}], \tag{1}$$

where $\rho^e$ is the electronic density and $\rho^{n_u}$ is the density for the $u$th type of nuclei.

In the multicomponent Kohn–Sham formalism, a non-interacting reference is introduced, which is assumed to have the same densities as the real interacting system. This non-interacting reference can be written as

$$|\Psi\rangle = |\Psi^e\rangle \prod_u |\Psi^{n_u}\rangle, \tag{2}$$

where $|\Psi^e\rangle$ is the electronic determinant and $|\Psi^{n_u}\rangle$ is the determinant or permanent of the $u$th type of nuclei, depending on its fermionic or bosonic nature. Then, electronic and nuclear densities can be obtained using their occupied orbitals,

$$\rho^e = \sum_i^{N^e} |\phi_i^e|^2, \tag{3}$$

$$\rho^{n_u} = \sum_I^{N^{n_u}} |\phi_I^{n_u}|^2, \tag{4}$$

in which $N^e$ is the number of electrons and $N^{n_u}$ is the number of nuclei of the $u$th type.

The total ground state energy can be expressed as a functional of both the electronic density and each type of nuclear density,

$$\begin{aligned} E[\rho^e, \{\rho^{n_u}\}] = &\left(T_s[\rho^e] + \sum_u T_s[\rho^{n_u}]\right) + \left(J^{ee}[\rho^e] + \sum_u J^{nn}[\rho^{n_u}]\right. \\ &\left. + \sum_u J^{en}[\rho^e, \rho^{n_u}] + \sum_u \sum_{v>u} J^{nn}[\rho^{n_u}, \rho^{n_v}]\right) \\ &+ \left(E_{xc}^e[\rho^e] + \sum_u E_{xc}^n[\rho^{n_u}]\right) + \left(E_{dpc}[\rho^e, \{\rho^{n_u}\}]\right) \\ &+ \left(E_{ext}^e[\rho^e] + \sum_u E_{ext}^n[\rho^{n_u}]\right), \end{aligned} \tag{5}$$

where the quantities in each parenthesis represent the kinetic energy of the non-interacting reference, mean-field Coulomb interaction energy, same-particle exchange-correlation energy, different-particle correlation energy, and external potential energy, respectively. In this full-quantum formulation, because all nuclei are treated quantum mechanically, the external potential energy terms vanish if there is no external field applied. Similar to conventional electronic density functional theory, this theory is also exact if the true (exchange-)correlation functionals are known.[21]

In practical chemical systems that we are interested in, some simplifications can be made based on the fact that the nuclei are relatively localized with little spatial overlap, which suggests that all the nuclei belonging to the same type can also be considered distinguishable. Therefore, the nuclear part of the Kohn–Sham reference can be approximated by a Hartree product of the orbital functions for each individual nucleus, regardless of their fermionic or bosonic nature,

$$|\Psi^e\rangle \prod_u |\Psi^{n_u}\rangle \approx |\Psi^e\rangle (|\phi_1^n\rangle \cdots |\phi_I^n\rangle \cdots |\phi_{N^n}^n\rangle) = |\Psi^e\rangle \prod_I^{N^n} |\phi_I^n\rangle, \tag{6}$$

where $N^n$ is the total number of nuclei. With this simplification, each nucleus is independently described by the corresponding

orbital function, which makes it possible to impose a constraint on each of them next.

In full-quantum cNEO-DFT, we impose a constraint on the expectation position for every nucleus,

$$\langle \phi_I^n | \mathbf{r} | \phi_I^n \rangle = \mathbf{R}_I. \tag{7}$$

With this constraint, each nucleus will be placed at a given position like in the Born–Oppenheimer picture, but the difference is that the nuclei here are described by orbital functions and their positions are the expectation values of the position operator.

Then, with this constraint as well as the orbital normalization requirement, the energy minimization can be carried out with the help of Lagrange multipliers. The Lagrangian function to be minimized is

$$\begin{aligned} L = E &+ \sum_I^{N^n} \mathbf{f}_I \cdot (\langle \phi_I^n | \mathbf{r} | \phi_I^n \rangle - \mathbf{R}_I) \\ &- \sum_i^{N^e} \epsilon_i^e (\langle \phi_i^e | \phi_i^e \rangle - 1) - \sum_I^{N^n} \epsilon_I^n (\langle \phi_I^n | \phi_I^n \rangle - 1), \end{aligned} \tag{8}$$

where $\mathbf{f}_I$ is the Lagrange multiplier and will later be proven to be the force acting on its corresponding nucleus. Minimizing the Lagrangian function leads to the electronic and nuclear Kohn–Sham equations,

$$\left( -\frac{1}{2}\nabla^2 + v_J^{ee} + v_J^{ne} + v_{xc}^e + v_{dpc}^e + v_{ext}^e \right) \phi_i^e = \epsilon_i^e \phi_i^e, \tag{9}$$

$$\left( -\frac{1}{2}\nabla^2 + v_J^{nn} + v_J^{en} + v_{xc}^n + v_{dpc}^n + v_{ext}^n + \mathbf{f}_I \cdot \mathbf{r} \right) \phi_I^n = \epsilon_I^n \phi_I^n, \tag{10}$$

where each term in the Fock operator on the left-hand side of the equations is obtained by taking the functional derivative of the corresponding energy term in Eq. (5) with respect to either the electron density or the nuclear density. In the nuclear equations, an extra term $\mathbf{f}_I \cdot \mathbf{r}$ shows up in the Fock operator due to the constraints applied on the expectation positions.

Equations (9) and (10) are coupled and can be solved iteratively if the proper set of $\{\mathbf{f}_I\}$ is known. However, in practice, the proper set of $\{\mathbf{f}_I\}$ that makes the nuclear orbitals satisfy Eq. (7) is unknown and also needs to be solved.

In our previous paper,[19] we proved that finding the proper $\mathbf{f}_I$ for Eq. (7) with a set of converged nuclear and electronic orbitals is equivalent to solving

$$\frac{\mathrm{d}L(\mathbf{f}_I)}{\mathrm{d}\mathbf{f}_I} = 0. \tag{11}$$

Therefore, an outer loop to search for the proper $\mathbf{f}_I$ is required. The whole procedure can be summarized in Fig. 1(a). However, this procedure is not very efficient because it requires the convergence of electron and proton orbitals for each updated $\mathbf{f}_I$. In this work, inspired by the optimization process in constrained DFT,[22] we adopt a more efficient procedure by placing the search for the proper $\mathbf{f}_I$ inside the nuclear loop. During the search, we directly target the $\mathbf{f}_I$ that satisfies Eq. (7) using root-finding algorithms. The new procedure can be summarized in Fig. 1(b), and it has been tested to be more efficient and robust in our calculations.

## B. Analytic gradient

In full-quantum cNEO-DFT, the positions of quantum nuclei are represented by the expectation positions of the nuclei. Therefore, the analytic gradient we will derive in the following is the response of the total cNEO-DFT energy with respect to the change of the expectation positions of the nuclei.

In the absence of any classical nuclei, the total energy has no explicit dependence on the quantum nuclear position, and the dependence is through the densities and, furthermore, the orbitals,

$$E(\mathbf{R}) = E(\boldsymbol{\phi}(\mathbf{R})). \tag{12}$$

The derivative of the energy with respect to the change of a nuclear expectation position is

$$\frac{\mathrm{d}E}{\mathrm{d}\mathbf{R}_I} = \sum_\phi \int \frac{\delta E}{\delta \phi} \frac{\mathrm{d}\phi}{\mathrm{d}\mathbf{R}_I} \mathrm{d}\mathbf{r} + \text{c.c.}, \tag{13}$$

where $\phi$ runs through all the electronic orbitals and nuclear orbitals and c.c. denotes the complex conjugate. In the case of a complete basis set,

$$\begin{aligned} \sum_\phi \int \frac{\delta E}{\delta \phi} \frac{\mathrm{d}\phi}{\mathrm{d}\mathbf{R}_I} \mathrm{d}\mathbf{r} + \text{c.c.} &= \left( \sum_{\phi^e} \int \phi^{e*} \hat{F}^e \frac{\mathrm{d}\phi^e}{\mathrm{d}\mathbf{R}_I} \mathrm{d}\mathbf{r} + \text{c.c.} \right) \\ &+ \left( \sum_{\phi_J^n} \int \phi_J^{n*} (\hat{F}^n - \mathbf{f}_J \cdot \mathbf{r}) \frac{\mathrm{d}\phi_J^n}{\mathrm{d}\mathbf{R}_I} \mathrm{d}\mathbf{r} + \text{c.c.} \right) \\ &= \sum_\phi \int \epsilon \frac{\mathrm{d}\langle \phi | \phi \rangle}{\mathrm{d}\mathbf{R}_I} \mathrm{d}\mathbf{r} - \sum_{\phi_J^n} \mathbf{f}_J \cdot \frac{\mathrm{d}\langle \phi_J^n | \mathbf{r} | \phi_J^n \rangle}{\mathrm{d}\mathbf{R}_I} \\ &= -\sum_{\phi_J^n} \mathbf{f}_J \delta_{IJ} = -\mathbf{f}_I, \end{aligned} \tag{14}$$

where $\hat{F}^e$ and $\hat{F}^n$ are the Fock operators defined on the left-hand side of Eqs. (9) and (10). This result indicates that the negative of the Lagrange multiplier is the gradient, and therefore, it can be perceived as the force acting on the corresponding quantum nucleus, which is the same as the single-proton cNEO-DFT case.

However, in practical numerical implementations with a finite basis set, the gradient derivation above is no longer strictly true. The electronic and nuclear molecular orbitals are both expressed in terms of a limited number of atomic orbitals that center at the nuclear expectation position $\mathbf{R}$,

$$\boldsymbol{\phi}(\mathbf{R}) = \boldsymbol{\varphi}(\mathbf{R}) \mathbf{C}(\mathbf{R}). \tag{15}$$

Here, we have used the compact matrix notation, in which $\boldsymbol{\varphi}(\mathbf{R})$ is a vector composed of atomic orbitals, $\boldsymbol{\phi}(\mathbf{R})$ is a vector composed of molecular orbitals, and $\mathbf{C}(\mathbf{R})$ is the molecular orbital coefficient matrix. Therefore, the energy dependence on the expectation position now should be perceived as

$$E(\mathbf{R}) = E(\boldsymbol{\phi}(\mathbf{R})) = E(\boldsymbol{\varphi}(\mathbf{R}), \mathbf{C}(\mathbf{R})). \tag{16}$$

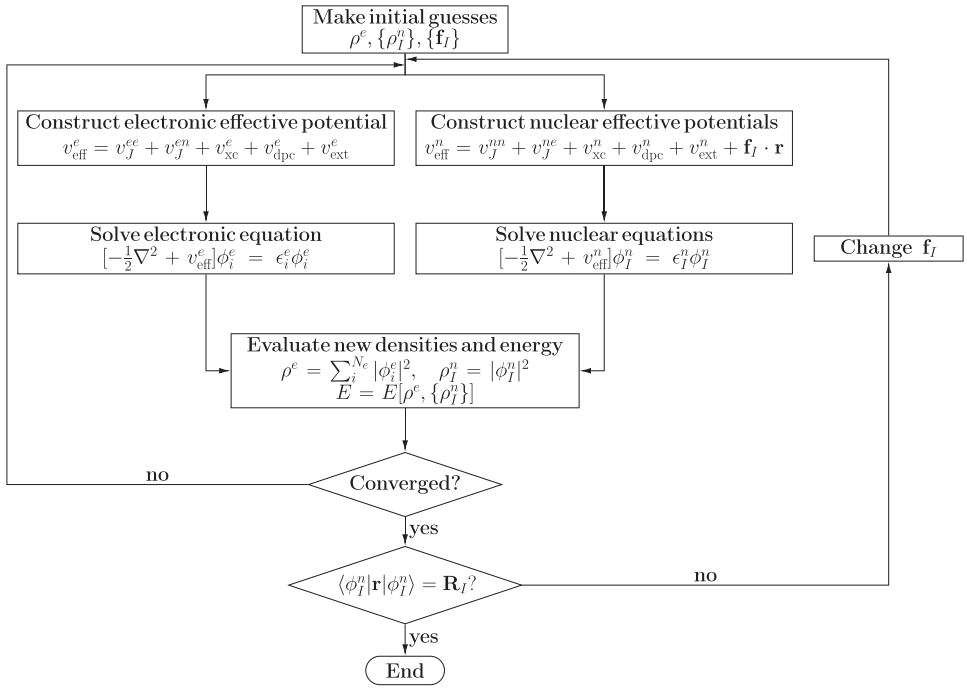


**FIG. 1.** Schematic representation for self-consistent loop structures for cNEO-DFT. The previous loop structure (a) solves $\{\mathbf{f}_I\}$ in an outer loop. The new loop structure (b) solves $\{\mathbf{f}_I\}$ in an inner loop, which has been tested to be more efficient and robust.

Then, the total derivative of the energy with respect to the change of a nuclear position is

$$\frac{\mathrm{d}E}{\mathrm{d}\mathbf{R}_I} = \left( \int \frac{\delta E}{\delta \boldsymbol{\varphi}} \frac{\mathrm{d}\boldsymbol{\varphi}}{\mathrm{d}\mathbf{R}_I} \mathrm{d}\mathbf{r} + \text{c.c.} \right) + \left( \mathrm{Tr}\left[ \frac{\partial E}{\partial \mathbf{C}} \frac{\mathrm{d}\mathbf{C}}{\mathrm{d}\mathbf{R}_I} \right] + \text{c.c.} \right). \tag{17}$$

The terms in the first parentheses are the dependence on $\mathbf{R}_I$ through $\boldsymbol{\varphi}$, and they can be evaluated directly when the energy is expressed in terms of atomic integrals involving $\varphi$ and density matrices. The terms in the second parentheses are the dependence on $\mathbf{R}_I$ through $\mathbf{C}$, and they require the dependence of $\mathbf{C}$ on $\mathbf{R}_I$, which is less straightforward to evaluate. The derivative of the energy with respect

to electronic coefficients and nuclear coefficients can be calculated independently,

$$\frac{\partial E}{\partial \mathbf{C}^e} = \mathbf{C}^{e\dagger}\mathbf{F}^e \tag{18}$$

and

$$\frac{\partial E}{\partial \mathbf{C}^n} = \mathbf{C}^{n\dagger}\mathbf{F}^n - \mathbf{C}^{n\dagger}\mathbf{f}^n \cdot \mathbf{r}^n, \tag{19}$$

where $\mathbf{F}^e$, $\mathbf{F}^n$, and $\mathbf{r}^n$ are the Fock matrix for electrons, the Fock matrix for nuclei, and the dipole matrix for nuclei, respectively, and $\mathbf{f}^n$ is a collection of the Lagrangian multipliers for the nuclei, i.e., $\mathbf{f}^n = (\mathbf{f}_1, \ldots, \mathbf{f}_I, \ldots, \mathbf{f}_{N^n})$. Again, the nuclear expression is different from the electronic expression because of the constraints applied. When combined with the response of $\mathbf{C}$ on $\mathbf{R}_I$, the electronic contributions to the second parentheses of Eq. (17) are

$$\begin{aligned}\mathrm{Tr}\left[\frac{\partial E}{\partial \mathbf{C}^e}\frac{\mathrm{d}\mathbf{C}^e}{\mathrm{d}\mathbf{R}_I}\right] + \text{c.c.} &= \mathrm{Tr}\left[\mathbf{C}^{e\dagger}\mathbf{F}^e\frac{\mathrm{d}\mathbf{C}^e}{\mathrm{d}\mathbf{R}_I}\right] + \text{c.c.} \\ &= \mathrm{Tr}\left[\epsilon^e\mathbf{C}^{e\dagger}\mathbf{S}^e\frac{\mathrm{d}\mathbf{C}^e}{\mathrm{d}\mathbf{R}_I}\right] + \text{c.c.} \\ &= -\mathrm{Tr}\left[\epsilon^e\mathbf{C}^{e\dagger}\frac{\mathrm{d}\mathbf{S}^e}{\mathrm{d}\mathbf{R}_I}\mathbf{C}^e\right]\end{aligned} \tag{20}$$

and the nuclear contributions are

$$\begin{aligned}\mathrm{Tr}\left[\frac{\partial E}{\partial \mathbf{C}^n}\frac{\mathrm{d}\mathbf{C}^n}{\mathrm{d}\mathbf{R}_I}\right] + \text{c.c.} &= \left(\mathrm{Tr}\left[\mathbf{C}^{n\dagger}\mathbf{F}^n\frac{\mathrm{d}\mathbf{C}^n}{\mathrm{d}\mathbf{R}_I}\right] + \text{c.c.}\right) \\ &\quad - \left(\mathrm{Tr}\left[\mathbf{C}^{n\dagger}\mathbf{f}^n\cdot\mathbf{r}^n\frac{\mathrm{d}\mathbf{C}^n}{\mathrm{d}\mathbf{R}_I}\right] + \text{c.c.}\right) \\ &= -\mathrm{Tr}\left[\epsilon^n\mathbf{C}^{n\dagger}\frac{\mathrm{d}\mathbf{S}^n}{\mathrm{d}\mathbf{R}_I}\mathbf{C}^n\right] \\ &\quad + \mathrm{Tr}\left[\mathbf{C}^{n\dagger}\mathbf{f}^n\cdot\frac{\mathrm{d}\mathbf{r}^n}{\mathrm{d}\mathbf{R}_I}\mathbf{C}^n\right] - \mathbf{f}_I.\end{aligned} \tag{21}$$

It can be seen that the expression for the electronic part is essentially the same as the analytic gradient in electronic DFT, which requires the gradient of the overlap matrix. In contrast, the expression for the nuclear part additionally requires the gradient of the dipole matrix as well as the Lagrange multiplier $-\mathbf{f}_I$, which has been shown in Eq. (14) to be the exact result in the complete basis set limit. For more details regarding the derivation and an expanded form for the final expression that is directly programmable, refer to the supplementary material.

## III. COMPUTATIONAL DETAILS

We implemented full-quantum cNEO-DFT and its analytic gradient in the PySCF package.[23] The correct implementation of the analytic gradient has been verified by the comparison with the finite-difference results. In all the test calculations, the B3LYP functional[24–26] was used to describe the electronic exchange-correlation. We chose this functional due to its popularity and generally good performance, but as was tested in previous literature,[27] the choice of electronic functionals should not make a big difference for multicomponent DFT calculations. Quantum nuclei were treated at the Hartree level with the self-interaction excluded. For qualitative illustration, we did not include any electron–nuclei or nuclei–nuclei correlation, although they may play an important role in an accurate quantitative description.[13,14] The electronic basis set was chosen to be cc-pVTZ,[28] whereas the even-tempered Gaussian basis set[29] was adopted for quantum nuclei with the exponents being $\alpha\beta^n$, in which the parameters $\alpha$ and $\beta$ vary based on the nuclear type. Specifically, the 8*s*8*p*8*d* basis set with $\alpha = 2\sqrt{2}$ and $\beta = \sqrt{2}$ was employed for protons, and the 12*s*12*p*12*d* basis sets were used for all the remaining nuclei with $\beta = \sqrt{3}$ and $\alpha = 4\sqrt{2}, 12\sqrt{2}, 14\sqrt{2}, 16\sqrt{2}$, and $18\sqrt{2}$ for D, C, N, O, and F, respectively. A detailed convergence test for nuclear basis sets can be found in the supplementary material. The energetic convergence for the self-consistent procedure of cNEO-DFT was set to be $10^{-8}$ hartree. In geometry optimizations, the molecular geometries were optimized until the maximal force on all atoms was less than 0.05 eV/Å by the Broyden–Fletcher–Goldfarb–Shanno (BFGS) algorithm implemented in the Atomic Simulation Environment (ASE) package.[30] The transition states were located by the dimer method[31] or the climbing-image nudged elastic band method.[32] The results were compared to DFT calculations with the same exchange-correlation functional and basis set as well as conventional NEO-DFT with only key proton treated quantum mechanically. In addition, DFT-VPT2[20] calculations were also performed for comparison using the Gaussian 16 package.[33]

## IV. RESULTS AND DISCUSSIONS

### A. Molecular energy and geometry

#### 1. Diatomic molecules

The conventional NEO method requires at least two classical nuclei to avoid the difficulties related to translations and rotations. In the full-quantum cNEO method, because the expectation positions of quantum nuclei are introduced, the molecular frame is fixed without translation or rotation. Therefore, the full-quantum cNEO method does not have the requirement on classical nuclei and is capable of describing both monoatomic and diatomic molecules.

The dissociation curves for $H_2$ and HF by unrestricted full-quantum cNEO-DFT are plotted in Fig. 2. The results are compared with conventional unrestricted DFT. It can be seen that all curves approach the correct zero dissociation limit at long interatomic distances. Conventional DFT does not distinguish isotopes and therefore gives the same dissociation curve for $H_2$/HD/$D_2$ as well as HF/DF. In contrast, the geometric isotope effect can be captured by the full-quantum cNEO-DFT as a result of the mass dependence in the nuclear kinetic term. Because the proton is lighter than the deuterium, among the hydrogen molecules, $H_2$ has the largest zero-point energy, whereas $D_2$ has the smallest. Similarly, HF has a larger zero-point energy than DF. Conventional DFT treats nuclei as point charges, which is essentially the same as performing a cNEO-DFT calculation with infinite nuclear mass. Therefore, conventional

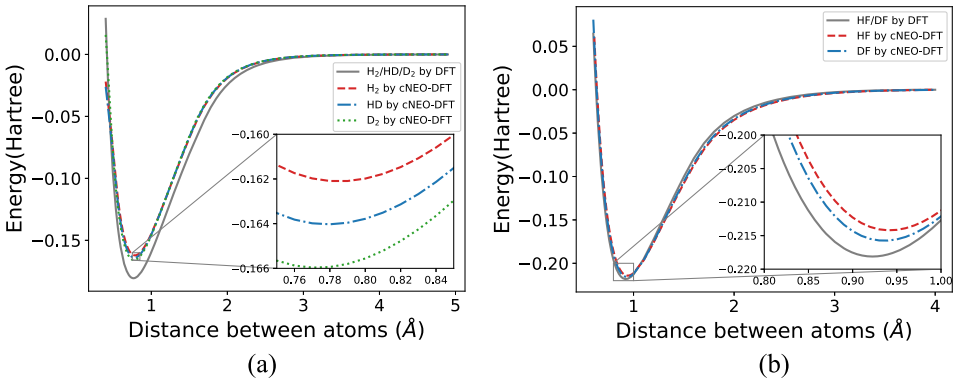


**FIG. 2.** Dissociation curves for (a) $H_2$/HD/$D_2$ and (b) HF/DF by DFT and full-quantum cNEO-DFT. The insets show the details around the equilibrium bond lengths.

DFT has no zero-point energy and thus gives the lowest total energy.

The insets of Figs. 2(a) and 2(b) show the details of the curves around the equilibrium bond lengths. Among the hydrogen molecules, $H_2$ has the longest equilibrium bond length, whereas $D_2$ has the shortest. Similarly, HF has a longer equilibrium bond length than DF. This is because cNEO-DFT provides a vibrationally averaged structure, which incorporates the anharmonic nature of the bonds by allowing light isotopes to have a higher probability to appear in the region with a long bond length. The quantitative results for the equilibrium bond lengths are listed in Table I and compared to DFT, DFT-VPT2, and experimental results. The equilibrium bond lengths from DFT-VPT2 are also from vibrationally averaged structures.[20] Therefore, the bond lengths from DFT-VPT2 and cNEO-DFT are all longer than the results from DFT. However, we observe that cNEO-DFT predicts slightly longer bond lengths than DFT-VPT2. The experimental values of the bond lengths have been corrected to eliminate the contributions from the vibrations; therefore, they correspond to equilibrium structures, which are close to DFT results and do not resemble DFT-VPT2 or full-quantum cNEO-DFT results.[34]

## 2. Linear polyatomic molecules

The equilibrium bond lengths of linear molecules $FHF^-$, HCN, and HNC are presented in Table II. The results of DFT-VPT2 are not available due to the difficulties in obtaining the average coordinates of linear polyatomic molecules.[36] Conventional NEO-DFT results are available for these molecules when only the hydrogen nucleus is treated quantum mechanically. Comparing the results from DFT and NEO-DFT, it can be seen that the nuclear quantum effects of hydrogen could lead to an increase of H–X bond by about 0.02 Å, in which X is a heavy atom, but they barely affect the lengths of the bonds between heavy atoms. Comparing the results from NEO-DFT and full-quantum cNEO-DFT, it can be seen that the nuclear quantum effects of heavier nuclei have a very small effect on the corresponding H–X bond length, which is an order of magnitude smaller than the effect of hydrogen. The lengths of the bonds between heavy atoms are also barely affected by the quantum effects of the involving nuclei.

## 3. Non-linear polyatomic molecules

Table III shows the equilibrium bond lengths of four non-linear molecules. Similar to the linear cases, the H–X bond lengths by DFT-VPT2 and full quantum cNEO-DFT are generally larger than those by DFT. However, in contrast, for the bonds between heavy atoms such as O–O and C–O, cNEO-DFT predicts similar or slightly

**TABLE I.** Bond lengths (in Å) of diatomic molecules.

| | Bond | Experiment[a] | DFT | DFT-VPT2 | Full-quantum cNEO-DFT |
|---|---|---|---|---|---|
| $H_2$ | H–H | 0.741 | 0.743 | 0.767 | 0.785 |
| HD | H-D | 0.741 | | 0.764 | 0.779 |
| $D_2$ | D–D | 0.742 | | 0.760 | 0.773 |
| HF | H–F | 0.917 | 0.922 | 0.938 | 0.942 |
| DF | D–F | ... | | 0.933 | 0.937 |

[a]Experimental data are from the National Institute of Standards and Technology (NIST) websites.

**TABLE II.** Bond lengths (in Å) of linear polyatomic molecules.

| | Bond | Experiment[a] | DFT | NEO-DFT | Full-quantum cNEO-DFT |
|---|---|---|---|---|---|
| $FHF^-$ | H–F | 1.138[b] | 1.149 | 1.164 | 1.162 |
| $FDF^-$ | D–F | ... | | 1.160 | 1.158 |
| HCN | C–H | 1.064 | 1.066 | 1.090 | 1.089 |
| | C–N | 1.156 | 1.147 | 1.147 | 1.147 |
| DCN | C–D | ... | 1.066 | 1.083 | 1.082 |
| | C–N | ... | 1.147 | 1.147 | 1.147 |
| HNC | N–H | 0.986 | 0.997 | 1.020 | 1.019 |
| | C–N | 1.173 | 1.165 | 1.165 | 1.165 |
| DNC | N–D | ... | 0.997 | 1.013 | 1.012 |
| | C–N | ... | 1.165 | 1.165 | 1.165 |

[a]The experimental data are from the National Institute of Standards and Technology (NIST) websites unless stated otherwise.
[b]Crystal structure results from Ref. 35.

**TABLE III**. Bond lengths (in Å) of non-linear molecules.

| | Bond | Experiment[a] | DFT | NEO-DFT | Full-quantum cNEO-DFT |
|---|---|---|---|---|---|
| $H_2O$ | H–O | 0.958 | 0.961 | 0.976 | 0.981 |
| HDO | H–O | 0.956 | | 0.975 | 0.982 |
| | D–O | 0.956 | | 0.973 | 0.975 |
| $D_2O$ | D–O | 0.956 | | 0.972 | 0.975 |
| $H_2O_2$ | H–O | 0.950 | 0.966 | 0.967 | 0.986 |
| | O–O | 1.475 | 1.452 | 1.463 | 1.448 |
| $H_2CO$ | C–H | 1.111 | 1.107 | 1.120 | 1.134 |
| | C–O | 1.205 | 1.199 | 1.203 | 1.198 |
| HCOOH | C–H | 1.097 | 1.096 | 1.106 | 1.123 |
| | C–O | 1.202 | 1.197 | 1.200 | 1.197 |
| | C–O | 1.343 | 1.345 | 1.352 | 1.341 |
| | O–H | 0.972 | 0.970 | 0.970 | 0.993 |

[a]The experimental data are from the National Institute of Standards and Technology (NIST) websites.

shorter bond lengths than DFT, whereas DFT-VPT2 also predicts longer bond lengths. Comparing the results of $H_2O$, HDO, and $D_2O$, we can see that the subtle hydrogen isotope effects on the bond lengths of water molecules can also be described by both DFT-VPT2 and full-quantum cNEO-DFT.

## B. Transition state energy and geometry

### 1. HCN/HNC and DCN/DNC isomerization

The geometries of the transition states and reaction barriers for the HCN/HNC and DCN/DNC isomerizations are presented in Table IV. Again, DFT cannot describe the geometric isotope effect and therefore gives the same results for the two reactions. Similar to the equilibrium molecular geometries, at transition states, the C–H(D) and N–H(D) bond lengths by DFT-VPT2, NEO-DFT, and full-quantum cNEO-DFT are also longer than those by DFT. NEO-DFT and full-quantum cNEO-DFT predict longer C–H(D) and N–H(D) bond lengths but shorter C–N bond lengths than DFT-VPT2. Comparing NEO-DFT and full quantum cNEO-DFT, it can be seen that the length of the N–H(D) bond can be reduced by 0.007 Å–0.008 Å when heavy atoms are also treated quantum mechanically, indicating the influence of the nuclear quantum effects for heavy nuclei in the description of transition states. The C–N bond lengths are very similar by DFT, NEO-DFT, and full-quantum cNEO-DFT, which is also in accordance with the results for bonds between heavy nuclei at equilibrium molecular geometries.

Nuclear quantum effects will lower the reaction barrier for the isomerization reaction, as shown in Table IV. Comparing NEO-DFT and full quantum cNEO-DFT, the inclusion of nuclear quantum effects for heavy atoms not only affects the transition state geometry but also significantly increases the reaction barrier of the HCN/HNC and DCN/DNC isomerization by about 1.0 kcal/mol.

### 2. Hydrogen transfer in 2-cyano-malondialdehyde

The results of a more complicated example, the hydrogen transfer in 2-cyano-malondialdehyde (cMDA), are shown in Table V. The key reaction region includes the two oxygen atoms and the one transferring hydrogen atom, so the distances between O(1)–H, O(2)–H, and O(1)–O(2) (Fig. 3) are investigated. In the NEO-DFT calculation, only the transferring H/D is treated quantum mechanically, whereas in full-quantum cNEO-DFT, all atoms are treated quantum mechanically. Comparing DFT and NEO-DFT, it can be seen that O(1)–H and O(1)–O(2) distances can change around 0.03 Å when nuclear quantum effects of the transfer H/D are taken into consideration. Further inclusion of the quantum effects of all nuclei leads to a change of about 0.01 Å for the O(1)–H and O(2)–H distances. This geometric change is larger than that in the HCN/HNC isomerization, and it indicates that the nuclear quantum effects for heavy atoms may be more significant in more complicated systems.

The reaction barrier for this reaction is only 2.9 kcal/mol by DFT, but it is reduced by about half when the nuclear quantum effects of the transferring H/D are taken into account in NEO-DFT. In full-quantum cNEO-DFT, the inclusion of nuclear quantum effects of heavy atoms further decreases the reaction barrier, although this change is not as significant as that by the hydrogen quantum effects. Previously, similar results have been found in the

**TABLE IV**. Geometries of transition states for HCN/HNC and DCN/DNC isomerization by cNEO and DFT.

| | | | DFT | DFT-VPT2 | NEO-DFT | Full-quantum cNEO-DFT |
|---|---|---|---|---|---|---|
| HCN/HNC | Distance (Å) | C–H | 1.189 | 1.203 | 1.214 | 1.215 |
| | | N–H | 1.390 | 1.401 | 1.419 | 1.412 |
| | | C–N | 1.181 | 1.186 | 1.180 | 1.179 |
| | Reaction barrier (kcal/mol) | | 47.57 | ... | 44.55 | 45.49 |
| DCN/DNC | Distance (Å) | C–D | 1.189 | 1.200 | 1.207 | 1.208 |
| | | N–D | 1.390 | 1.398 | 1.411 | 1.403 |
| | | C–N | 1.181 | 1.185 | 1.180 | 1.180 |
| | Reaction barrier (kcal/mol) | | 47.57 | ... | 45.43 | 46.37 |

**TABLE V**. Geometries of transition states for the proton transfer in cMDA.

| | | | DFT | DFT-VPT2 | NEO-DFT | Full-quantum cNEO-DFT |
|---|---|---|---|---|---|---|
| cMDA | Distance (Å) | O(1)–H | 1.226 | 1.239 | 1.253 | 1.262 |
| | | O(2)–H | 1.198 | 1.218 | 1.203 | 1.192 |
| | | O(1)–O(2) | 2.376 | 2.403 | 2.401 | 2.398 |
| | Reaction barrier (kcal/mol) | | 2.887 | ... | 1.035 | 1.010 |
| cMDA(D) | Distance (Å) | O(1)–D | 1.226 | 1.236 | 1.248 | 1.259 |
| | | O(2)–D | 1.198 | 1.211 | 1.199 | 1.190 |
| | | O(1)–O(2) | 2.376 | 2.395 | 2.393 | 2.394 |
| | Reaction barrier (kcal/mol) | | 2.887 | ... | 1.481 | 1.475 |

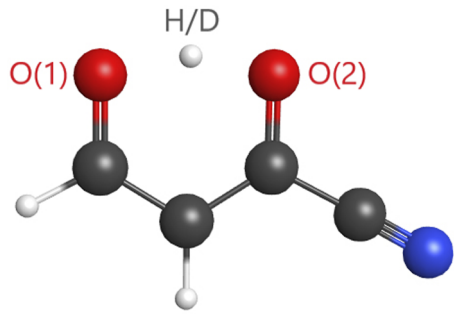


**FIG. 3**. The cMDA molecule.

literature that in the intramolecule proton transfer in malondialdehyde, the quantum nature of the heavy atoms that simply serve as a molecular frame also has a non-negligible impact on the free-energy barrier.[37]

## V. CONCLUSIONS

We developed the full-quantum formulation of cNEO-DFT by applying a constraint on the expectation position for every nucleus. It deviates from the conventional Born–Oppenheimer framework, and all nuclei and electrons are simultaneously described within the molecular orbital picture. The similarities and differences between this full-quantum cNEO-DFT and the conventional BO picture can be summarized as follows:

(1) Both theories have positions assigned to nuclei, which set the molecular frame and avoid the treatment on translations and rotations. However, the conventional BO picture uses the positions of nuclear point charges, whereas full-quantum cNEO-DFT uses the expectation positions of nuclear densities.
(2) The BO treatment first describes electrons quantum mechanically while treating nuclei as point charges and then can describe the nuclei quantum mechanically using the potential energy surface obtained. In contrast, the full-quantum cNEO-DFT simultaneously treats all particles quantum mechanically, and therefore, the electrons directly feel the potential from the delocalized quantum nuclei.
(3) Both methods have an energy profile. However, the potential energy surface obtained from the BO treatment does not include zero-point energies, whereas the full-quantum cNEO-DFT gives the total energy, which inherently includes the vibrational zero-point energies.
(4) The full-quantum cNEO-DFT reduces to the conventional multicomponent DFT when the Lagrange multipliers **f** vanish, which is in principle exact for a chemical system if the exact functionals are known. In contrast, a pure BO approximation is far from being exact: the separate treatment of electrons and nuclei makes it further need the diagonal Born–Oppenheimer correction as well as the challenging nonadiabatic coupling terms, which is often derived starting from a Born–Huang ansatz.

The full-quantum cNEO-DFT naturally overcomes the limitation of convention NEO-DFT that requires at least two classical atoms to avoid the problems related to translations and rotations. It also includes all zero-point energies in its total energy and therefore gives higher energies than conventional DFT. In this work, the analytic gradient for full-quantum cNEO-DFT was also derived and applied to the geometry optimization and transition state search. Our tests on a series of small molecules and two proton transfer reactions by DFT, DFT-VPT2, conventional NEO-DFT, and full-quantum cNEO-DFT showed that the cNEO-DFT has similar effects to DFT-VPT2: They both provide vibrationally averaged structures and therefore usually predict longer bond lengths for bonds with significant anharmonicity. The quantum effects of hydrogen can have a non-negligible impact on the molecular equilibrium species as well as transition states. In complicated systems, such as the transition state of the cMDA, the nuclear quantum effects of heavy atoms may also be significant with a notable impact on the transition state geometries and reaction barriers. Apart from the geometric isotope effects in this work, future studies may apply the full-quantum cNEO-DFT to the study of kinetic isotope effects, and this method may be promising in the investigation of the nuclear quantum effects in a variety of chemical processes.

## SUPPLEMENTARY MATERIAL

See the supplementary material for a detailed derivation of the analytic gradient for the full-quantum cNEO-DFT as well as the convergence test for nuclear basis sets.

## ACKNOWLEDGMENTS

We are grateful for the support and funding from the University of Wisconsin via the Wisconsin Alumni Research Foundation.

## DATA AVAILABILITY

The data that support the findings of this study are available within the article and its supplementary material.

## REFERENCES

[1] S. Matsika and P. Krause, Annu. Rev. Phys. Chem. **62**, 621 (2011).
[2] A. Abedi, N. T. Maitra, and E. K. U. Gross, Phys. Rev. Lett. **105**, 123002 (2010).
[3] T. Yonehara, K. Hanasaki, and K. Takatsuka, Chem. Rev. **112**, 499 (2012).
[4] S. Habershon, D. E. Manolopoulos, T. E. Markland, and T. F. Miller, Annu. Rev. Phys. Chem. **64**, 387 (2013).
[5] B. F. E. Curchod and T. J. Martínez, Chem. Rev. **118**, 3305 (2018).
[6] F. Agostini and B. F. E. Curchod, Wiley Interdiscip. Rev.: Comput. Mol. Sci. **9**, e1417 (2019).
[7] S. P. Webb, T. Iordanov, and S. Hammes-Schiffer, J. Chem. Phys. **117**, 4106 (2002).
[8] H. Nakai, Int. J. Quantum Chem. **107**, 2849 (2007).
[9] T. Ishimoto, M. Tachikawa, and U. Nagashima, Int. J. Quantum Chem. **109**, 2677 (2009).
[10] F. Pavošević, T. Culpitt, and S. Hammes-Schiffer, Chem. Rev. **120**, 4222 (2020).
[11] I. L. Thomas, Phys. Rev. **185**, 90 (1969).
[12] A. Sirjoosingh, M. V. Pak, K. R. Brorsen, and S. Hammes-Schiffer, J. Chem. Phys. **142**, 214107 (2015).
[13] Y. Yang, K. R. Brorsen, T. Culpitt, M. V. Pak, and S. Hammes-Schiffer, J. Chem. Phys. **147**, 114113 (2017).
[14] K. R. Brorsen, Y. Yang, and S. Hammes-Schiffer, J. Phys. Chem. Lett. **8**, 3488 (2017).
[15] Y. Yang, T. Culpitt, and S. Hammes-Schiffer, J. Phys. Chem. Lett. **9**, 1765 (2018).
[16] F. Pavošević, T. Culpitt, and S. Hammes-Schiffer, J. Chem. Theory Comput. **15**, 338 (2019).
[17] T. Iordanov and S. Hammes-Schiffer, J. Chem. Phys. **118**, 9489 (2003).
[18] Y. Yang, P. E. Schneider, T. Culpitt, F. Pavošević, and S. Hammes-Schiffer, J. Phys. Chem. Lett. **10**, 1167 (2019).
[19] X. Xu and Y. Yang, J. Chem. Phys. **152**, 084107 (2020).
[20] V. Barone, J. Chem. Phys. **122**, 014108 (2004).
[21] J. F. Capitani, R. F. Nalewajski, and R. G. Parr, J. Chem. Phys. **76**, 568 (1982).
[22] Q. Wu and T. Van Voorhis, Phys. Rev. A **72**, 024502 (2005).
[23] Q. Sun, T. C. Berkelbach, N. S. Blunt, G. H. Booth, S. Guo, Z. Li, J. Liu, J. D. McClain, E. R. Sayfutyarova, S. Sharma, S. Wouters, and G. K.-L. Chan, Wiley Interdiscip. Rev.: Comput Mol Sci **8**, e1340 (2018).
[24] A. D. Becke, Phys. Rev. A **38**, 3098 (1988).
[25] C. Lee, W. Yang, and R. G. Parr, Phys. Rev. B **37**, 785 (1988).
[26] A. D. Becke, J. Chem. Phys. **98**, 5648 (1993).
[27] K. R. Brorsen, P. E. Schneider, and S. Hammes-Schiffer, J. Chem. Phys. **149**, 044110 (2018).
[28] T. H. Dunning, J. Chem. Phys. **90**, 1007 (1989).
[29] R. D. Bardo and K. Ruedenberg, J. Chem. Phys. **60**, 918 (1974).
[30] A. H. Larsen, J. J. Mortensen, J. Blomqvist, I. E. Castelli, R. Christensen, M. Dułak, J. Friis, M. N. Groves, B. Hammer, C. Hargus, E. D. Hermes, P. C. Jennings, P. B. Jensen, J. Kermode, J. R. Kitchin, E. L. Kolsbjerg, J. Kubal, K. Kaasbjerg, S. Lysgaard, J. B. Maronsson, T. Maxson, T. Olsen, L. Pastewka, A. Peterson, C. Rostgaard, J. Schiøtz, O. Schütt, M. Strange, K. S. Thygesen, T. Vegge, L. Vilhelmsen, M. Walter, Z. Zeng, and K. W. Jacobsen, J. Phys.: Condens. Matter **29**, 273002 (2017).
[31] G. Henkelman and H. Jónsson, J. Chem. Phys. **111**, 7010 (1999).
[32] G. Henkelman, B. P. Uberuaga, and H. Jónsson, J. Chem. Phys. **113**, 9901 (2000).
[33] M. J. Frisch, G. W. Trucks, H. B. Schlegel, G. E. Scuseria, M. A. Robb, J. R. Cheeseman, G. Scalmani, V. Barone, G. A. Petersson, H. Nakatsuji, X. Li, M. Caricato, A. V. Marenich, J. Bloino, B. G. Janesko, R. Gomperts, B. Mennucci, H. P. Hratchian, J. V. Ortiz, A. F. Izmaylov, J. L. Sonnenberg, D. Williams-Young, F. Ding, F. Lipparini, F. Egidi, J. Goings, B. Peng, A. Petrone, T. Henderson, D. Ranasinghe, V. G. Zakrzewski, J. Gao, N. Rega, G. Zheng, W. Liang, M. Hada, M. Ehara, K. Toyota, R. Fukuda, J. Hasegawa, M. Ishida, T. Nakajima, Y. Honda, O. Kitao, H. Nakai, T. Vreven, K. Throssell, J. A. Montgomery, Jr., J. E. Peralta, F. Ogliaro, M. J. Bearpark, J. J. Heyd, E. N. Brothers, K. N. Kudin, V. N. Staroverov, T. A. Keith, R. Kobayashi, J. Normand, K. Raghavachari, A. P. Rendell, J. C. Burant, S. S. Iyengar, J. Tomasi, M. Cossi, J. M. Millam, M. Klene, C. Adamo, R. Cammi, J. W. Ochterski, R. L. Martin, K. Morokuma, O. Farkas, J. B. Foresman, and D. J. Fox, Gaussian 16 Revision C.01, Gaussian, Inc., Wallingford, CT, 2016.
[34] F. Pawłowski, P. Jørgensen, J. Olsen, F. Hegelund, T. Helgaker, J. Gauss, K. L. Bak, and J. F. Stanton, J. Chem. Phys. **116**, 6482 (2002).
[35] W. A. Denne and M. F. Mackay, J. Cryst. Mol. Struct. **1**, 311 (1971).
[36] Y. Morino, K. Kuchitsu, and T. Shimanouchi, J. Chem. Phys. **20**, 726 (1952).
[37] M. E. Tuckerman and D. Marx, Phys. Rev. Lett. **86**, 4946 (2001).